

**Astrophysical ${}^3\text{He}(\alpha, \gamma){}^7\text{Be}$ and ${}^3\text{H}(\alpha, \gamma){}^7\text{Li}$ direct capture reactions
in a potential model approach**

E. M. Tursunov* and S. A. Turakulov†

*Institute of Nuclear Physics, Academy of Sciences,
100214, Ulugbek, Tashkent, Uzbekistan*

A. S. Kadyrov‡

*Curtin Institute for Computation and Department of Physics and Astronomy,
Curtin University, GPO Box U1987, Perth, WA 6845, Australia*

Abstract

The astrophysical ${}^3\text{He}(\alpha, \gamma){}^7\text{Be}$ and ${}^3\text{H}(\alpha, \gamma){}^7\text{Li}$ direct capture processes are studied in the framework of the two-body model with the potentials of a simple Gaussian form, which describe correctly the phase-shifts in the s-, p-, d-, and f-waves, as well as the binding energy and the asymptotic normalization constant of the ground $p_{3/2}$ and the first excited $p_{1/2}$ bound states. It is shown that the E1-transition from the initial s-wave to the final p-waves is strongly dominant in both capture reactions. On this basis the s-wave potential parameters are adjusted to reproduce the new data of the LUNA collaboration around 100 keV and the newest data at the Gamov peak estimated with the help of the observed neutrino fluxes from the Sun, $S_{34}(23_{-5}^{+6} \text{ keV})=0.548\pm 0.054$ keV b for the astrophysical S-factor of the capture process ${}^3\text{He}(\alpha, \gamma){}^7\text{Be}$. The resulting model describes well the astrophysical S-factor in low-energy Big Bang nucleosynthesis region of 180-400 keV, however has a tendency to underestimate the data above 0.5 MeV. The energy dependence of the S-factor is mostly consistent with the data and the results of the no-core shell model with continuum, but substantially different from the fermionic molecular dynamics model predictions. Two-body potentials, adjusted on the properties of the ${}^7\text{Be}$ nucleus, ${}^3\text{He} + \alpha$ elastic scattering data and the astrophysical S-factor of the ${}^3\text{He}(\alpha, \gamma){}^7\text{Be}$ direct capture reaction, are able to reproduce the properties of the ${}^7\text{Li}$ nucleus, the binding energies of the ground $3/2^-$ and first excited $1/2^-$ states, and phase shifts of the ${}^3\text{H} + \alpha$ elastic scattering in partial waves. Most importantly, these potential models can successfully describe both absolute value and energy dependence of the existing experimental data for the mirror astrophysical ${}^3\text{H}(\alpha, \gamma){}^7\text{Li}$ capture reaction without any additional adjustment of the parameters.

PACS numbers: 11.10.Ef, 12.39.Fe, 12.39.Ki

* tursune@inp.uz

† turakulov@inp.uz

‡ a.kadyrov@curtin.edu.au

I. INTRODUCTION

The radiative capture ${}^3\text{He}(\alpha, \gamma){}^7\text{Be}$ and ${}^3\text{H}(\alpha, \gamma){}^7\text{Li}$ processes are the key nuclear reactions in stellar nucleosynthesis [1, 2]. Both of these reactions are important for studies of the primordial nucleosynthesis, in particular, for the solution of the so-called ${}^7\text{Li}$ abundance problem [3]. In addition, the ${}^3\text{He}(\alpha, \gamma){}^7\text{Be}$ reaction is very useful for the study of the kinetics of processes taking place in the Sun since it is a starting point for the second and third chains in the pp -cycle of hydrogen burning. On the other hand the ${}^7\text{Be}$ nucleus plays a dominant role in the neutrino production processes in both solar and Big Bang nucleosynthesis (BBN) models.

Experimental studies of the ${}^3\text{He}(\alpha, \gamma){}^7\text{Be}$ and ${}^3\text{H}(\alpha, \gamma){}^7\text{Li}$ radiative capture processes started in 1960s [4, 5]. Since then these reactions have consistently attracted interest of experimentalists [6–11]. Recent measurements were reported in [12–19]. The main difficulty in laboratory studies of these processes at low energies of astrophysical relevance (roughly from 20 to 500 keV) is related with the presence of strong Coulomb repulsive forces, especially for the production of the ${}^7\text{Be}$ nucleus. Due to this difficulty the measured values of the astrophysical S-factor contain large uncertainties. The most accurate experimental results for the astrophysical S-factor were obtained by the LUNA collaboration [13, 14] in a low-energy region around $E_{\text{cm}}=100$ keV, where E_{cm} is the collision energy in the center of mass (cm) frame. The experimental uncertainties in the measured values of the astrophysical S-factor around 70 keV b are much smaller than those in the old data. However, even these smaller error bars can have a strong influence on estimations of the astrophysical reaction rates in the BBN and solar models [1]. Therefore, there is still a need for more accurate experimental studies in the low energy region.

Very recently observed neutrino fluxes from the Sun were used to estimate the ${}^3\text{He}(\alpha, \gamma){}^7\text{Be}$ astrophysical S-factor within the standard solar model at the Gamow peak to be $S_{34}(23_{-5}^{+6}$ keV) $=0.548\pm 0.054$ keV b [20]. This new data point was then used for evaluation of the astrophysical S-factor at Big Bang energies and the corresponding thermonuclear reaction rates. However, an estimate of the primordial lithium abundance, ${}^7\text{Li}/\text{H}=5\times 10^{-10}$, obtained in the model is much larger than the observed Spite plateau [2].

From the theoretical side, potential models [21–23], microscopic R-matrix approach [24], microscopic cluster models [25, 26], microscopic approach based on an algebraic version of

the resonating group method [27], fermionic molecular dynamics (FMD) method [28], no-core shell model with continuum (NCSMC) [29] and the semimicroscopic phenomenological approach [30] have been developed to study the astrophysical ${}^3\text{He}(\alpha, \gamma){}^7\text{Be}$ and ${}^3\text{H}(\alpha, \gamma){}^7\text{Li}$ reactions. The most elaborate microscopic approaches based on the NCSMC and FMD yield an overall good description of the experimental data except the old data from Ref. [5] which are now believed to be less accurate. However the astrophysical S-factor obtained within these two methods show different energy dependence for both capture processes. At the same time they describe well the data of the LUNA collaboration [13, 14] and the newest data coming from the observed neutrino flux at the Gamov peak [20]. One should note that a fully ab-initio calculation of these radiative capture reactions, including three-body nuclear forces is not yet available and is still a big challenge. On the other hand, the question whether or not a simple potential model is able to reproduce the available data for the capture reactions at least in the BBN energy region of $E_{\text{cm}}=180\text{-}400$ keV remains to be answered. How does the description of the data for the astrophysical S-factor compare with the corresponding ab-initio results? To our best knowledge, these questions are still open. The most realistic potential model [22] based on folding potentials agrees well with the old data [5], which is much lower than the new data from Refs.[13, 14] at the astrophysical, low energy region.

Potential cluster models are able to reproduce both the bound state properties and the scattering data [21, 31]. An important feature of the potential models is that the two-body potentials have to be adjusted to reproduce not only the phase shifts in all partial waves and the binding energies of the bound states, but also the asymptotic properties of the bound state wave functions, like the asymptotic normalization coefficient (ANC). The importance of asymptotic properties of the two-body potentials have been demonstrated for the astrophysical $\alpha(d, \gamma){}^6\text{Li}$ capture process at low energies [32, 33]. Required empirical values of the asymptotic normalization coefficient can be extracted from the scattering data within different approaches, e.g. analytic continuation to the S-matrix pole [34], the effective range method [35–37] and distorted-wave Born approximation (DWBA) [38].

The potential models can also be used to improve the accuracy of the direct experiments on astrophysical capture reactions. Recently, a photon angular distribution calculated in the potential model has been used [39] to find the best kinematic conditions for the measurement of the ${}^2\text{H}(\alpha, \gamma){}^6\text{Li}$ reaction.

The aim of present paper is to study in detail the astrophysical ${}^3\text{He}(\alpha, \gamma){}^7\text{Be}$ and ${}^3\text{H}(\alpha, \gamma){}^7\text{Li}$ capture reactions in a potential model. As it is known from the literature, and as will be seen below, the most important contribution to above processes at low astrophysical energies comes from the dipole E1-transition operator, while the E2-transition only gives a small contribution in the resonance energy region. The M1-transition is also strongly suppressed. The two-body Gaussian potentials [21] which reproduce the bound states energies and the phase shifts in each partial wave will be examined. The potential parameters will be adjusted to reproduce the empirical values of the asymptotic normalization coefficient in the $p_{3/2}$ - and $p_{1/2}$ -bound states of the ${}^7\text{Be}$ nucleus, recently extracted from the phase-shift analysis within the DWBA method [38] and from the analysis of the experimental S-factor [40]. The d- and f-wave potentials from Ref. [21], which describe the corresponding phase shifts well, will be applied.

As the E1-transition occurs from the initial s-wave scattering state to the final p-wave bound states, the choice of the s-wave potentials is the next most important point of the potential model. The existence of infinite number of phase-equivalent potentials opens a unique possibility to adjust the S-wave potential parameters to the experimental astrophysical S-factor. The nodal positions of the s-wave scattering wave function, as well as the p-wave bound state wave functions at short distances due to their orthogonality to the Pauli forbidden states (two in s-wave and one in each of the partial $p_{1/2}$ and $p_{3/2}$ -waves) play a crucial role in decreasing effective overlap integrals, involving these two wave functions, thus resulting in the low values of the astrophysical S-factor, consistent with the experimental results. In this sense a role of the Pauli forbidden states in the capture process is similar to that in the beta-decay of the ${}^6\text{He}$ halo nucleus into the $\alpha - d$ continuum [41, 42].

At the first step the initial potential from Ref. [21] will be examined in the s-wave. After that we will show that it is possible to find the most suitable model among the phase-equivalent potentials, fitting the s-wave potential parameters to the astrophysical S-factor of the LUNA collaboration [13, 14] and the newest data at the Gamov peak [20] in low energy region. The astrophysical S-factor of the mirror reaction ${}^3\text{H}(\alpha, \gamma){}^7\text{Li}$ will be estimated with the same potentials, constructed from the study of the ${}^3\text{He}(\alpha, \gamma){}^7\text{Be}$ capture process by appropriate modification of the Coulomb interaction potential due to the difference in the charge values of the clusters ${}^3\text{He}$ and ${}^3\text{H}$.

The theoretical model will be briefly described in Section II, numerical results will be

given in Section III, and conclusions will be drawn in the last section.

II. THEORETICAL MODEL

A. Wave functions

In a single channel approximation, the initial and final state wave functions are defined as

$$\Psi_{lS}^J = \frac{u_E^{(lSJ)}(r)}{r} \{Y_l(\hat{r}) \otimes \chi_S(\xi)\}_{JM} \quad (1)$$

and

$$\Psi_{l_f S}^{J_f} = \frac{u^{(l_f S J_f)}(r)}{r} \{Y_{l_f}(\hat{r}) \otimes \chi_S(\xi)\}_{J_f M_f}, \quad (2)$$

respectively. The radial wave functions of the initial α - ^3He and α - ^3H scattering states in the $s_{1/2}$, $p_{1/2}$, $p_{3/2}$, $d_{3/2}$, $d_{5/2}$, $f_{5/2}$, $f_{7/2}$ partial waves are found as solutions of the two-body Schrödinger equation

$$\left[-\frac{\hbar^2}{2\mu} \left(\frac{d^2}{dr^2} - \frac{l(l+1)}{r^2} \right) + V^{lSJ}(r) \right] u_E^{(lSJ)}(r) = E u_E^{(lSJ)}(r), \quad (3)$$

where μ is the reduced mass of the clusters involved in the capture process, $1/\mu = 1/m_1 + 1/m_2$, and $V^{lSJ}(r)$ is a two-body potential in the partial wave with the orbital momentum l , spin S and total momentum J . The wave functions $u^{(l_f S J_f)}(r)$ of the final $p_{3/2}$ ground and $p_{1/2}$ excited bound states are found as solutions of the bound-state Schrödinger equation. For the solution of the Schrödinger equation the Numerov algorithm of a high accuracy of order $O(\hbar^6)$ is applied. The calculated wave functions allow one to estimate the characteristics of the astrophysical capture reactions $^3\text{He}(\alpha, \gamma)^7\text{Be}$ and $^3\text{H}(\alpha, \gamma)^7\text{Li}$, the cross section and the astrophysical S-factor.

The radial scattering wave function is normalized with the help of the asymptotic relation

$$u_E^{(lSJ)}(r) \xrightarrow{r \rightarrow \infty} \cos \delta_{lSJ}(E) F_l(\eta, kr) + \sin \delta_{lSJ}(E) G_l(\eta, kr), \quad (4)$$

where k is the wave number of the relative motion, η is the Zommerfeld parameter, F_l and G_l are regular and irregular Coulomb functions, respectively, and $\delta_{lSJ}(E)$ is the phase shift in the (l, S, J) th partial wave.

The α - ^3He and α - ^3H two-body potentials are taken in a simple Gaussian form [21]:

$$V^{lSJ}(r) = V_0 \exp(-\alpha r^2) + V_c(r), \quad (5)$$

where the Coulomb part is given as

$$V_c(r) = \begin{cases} Z_1 Z_2 e^2 / r & \text{if } r > R_c, \\ Z_1 Z_2 e^2 (3 - r^2 / R_c^2) / (2R_c) & \text{otherwise,} \end{cases} \quad (6)$$

with the Coulomb parameter R_c , and charge numbers Z_1, Z_2 of the first and second clusters, respectively. The parameters α, V_0 and R_c of the potential are specified for each partial wave.

B. Cross sections of the radiative capture process

The cross sections of the radiative capture process read [21, 43]

$$\sigma(E) = \sum_{J_f \lambda \Omega} \sigma_{J_f \lambda}(\Omega), \quad (7)$$

where $\Omega = \text{E}$ or M (electric or magnetic transition), λ is a multiplicity of the transition, J_f is the total angular momentum of the final state. For a particular final state with total momentum J_f and multiplicity λ we have

$$\begin{aligned} \sigma_{J_f \lambda}(\Omega) &= \sum_J \frac{(2J_f + 1)}{[S_1][S_2]} \frac{32\pi^2(\lambda + 1)}{\hbar \lambda ([\lambda]!!)^2} k_\gamma^{2\lambda+1} C^2(S) \\ &\times \sum_{lS} \frac{1}{k_i^2 v_i} | \langle \Psi_{l_f S}^{J_f} \| M_\lambda^\Omega \| \Psi_{lS}^J \rangle |^2, \end{aligned} \quad (8)$$

where l, l_f are the orbital momenta of the initial and final states, respectively, k_i and v_i are the wave number and velocity of the α - ^3He (or α - ^3H) relative motion of the entrance channel, respectively; S_1, S_2 are spins of the clusters α and ^3He (or ^3H), $k_\gamma = E_\gamma / \hbar c$ is the wave number of the photon corresponding to energy $E_\gamma = E_{\text{th}} + E$, where E_{th} is the threshold energy. Constant $C^2(S)$ is the spectroscopic factor [43]. As it was argued in Ref.[44], within the potential approach its value must be taken equal to 1 if the phase shifts in the partial waves are correctly reproduced. We also use short-hand notations $[S] = 2S + 1$ and $[\lambda]!! = (2\lambda + 1)!!$.

The reduced matrix elements are evaluated between the initial and final states represented by wave functions Ψ_{lS}^J and $\Psi_{l_f S}^{J_f}$, respectively.

The electric transition operator in the long-wavelength approximation reads

$$M_{\lambda m}^E = e \sum_{j=1}^A Z_j r_j'^{\lambda} Y_{\lambda m}(\hat{r}'_j), \quad (9)$$

where $\vec{r}'_j = \vec{r}_j - \vec{R}_{cm}$ is the radius vector of the j th particle in the center of mass system. Its reduced matrix elements can be evaluated as follows:

$$\begin{aligned} \langle \Psi_{l_f S}^{J_f} \| M_{\lambda}^E \| \Psi_{l S}^J \rangle &= e \left[Z_1 \left(\frac{A_2}{A} \right)^{\lambda} + Z_2 \left(\frac{-A_1}{A} \right)^{\lambda} \right] \\ &\times (-1)^{J+l+S} \left(\frac{[\lambda][l][J]}{4\pi} \right)^{1/2} C_{\lambda 0 l 0}^{l_f 0} \left\{ \begin{array}{ccc} J & l & S \\ l_f & J_f & \lambda \end{array} \right\} \int_0^{\infty} u_E^{(l S J)}(r) r^{\lambda} u^{(l_f S J_f)}(r) dr, \end{aligned} \quad (10)$$

where A_1, A_2 are mass numbers of the clusters in the entrance channel, $A = A_1 + A_2$.

The magnetic transition operator reads

$$\begin{aligned} M_{1\mu}^M &= \sqrt{\frac{3}{4\pi}} \left[\sum_{j=1}^A \mu_N \frac{Z_j}{A_j} \hat{l}_{j\mu} + 2\mu_j \hat{S}_{j\mu} \right] \\ &= \sqrt{\frac{3}{4\pi}} \left[\mu_N \left(\frac{A_2 Z_1}{A A_1} + \frac{A_1 Z_2}{A A_2} \right) \hat{l}_{r\mu} + 2(\mu_1 \hat{S}_{1\mu} + \mu_2 \hat{S}_{2\mu}) \right], \end{aligned} \quad (11)$$

where μ_N is the nuclear magneton, μ_j is the magnetic moment and $\hat{l}_{j\mu}$ is the orbital momentum of j th particle. The angular momentum of the relative motion is denoted as $\hat{l}_{r\mu}$. The reduced matrix elements of the magnetic M1 transition operator can be evaluated as

$$\begin{aligned} \langle \Psi_{l_f S}^{J_f} \| M_1^M \| \Psi_{l S}^J \rangle &= \mu_N \left(\frac{A_2 Z_1}{A A_1} + \frac{A_1 Z_2}{A A_2} \right) \sqrt{l_f(l_f + 1)[J_f][l_f]} (-1)^{S+1+J_f+l_f} \left\{ \begin{array}{ccc} l_f & S & J_f \\ J & 1 & l_f \end{array} \right\} I_{if} \\ &+ 2\mu(^3\text{He}) (-1)^{1+l_f+3S-J} \sqrt{S(S+1)[S][J_f]} \left\{ \begin{array}{ccc} S & l_f & J_f \\ J & 1 & S \end{array} \right\} I_{if}, \end{aligned} \quad (12)$$

where the overlap integral is given as

$$I_{if} = \delta_{l_f} \sqrt{\frac{3}{4\pi}} \int_0^{\infty} u_E^{(l S J)}(r) u^{(l_f S J_f)}(r) dr. \quad (13)$$

In addition, $\mu(^3\text{He}) = -2.1275 \mu_N$ is the magnetic momentum of the ^3He nucleus, which must be replaced by the magnetic momentum $\mu(^3\text{H}) = 2.979 \mu_N$ of the ^3H nucleus for the mirror reaction.

Finally, the astrophysical S -factor of the process is expressed in terms of the cross section as [45]

$$S(E) = E \sigma(E) \exp(2\pi\eta). \quad (14)$$

III. NUMERICAL RESULTS

A. Details of the calculations and phase-shift descriptions

For the solution of the Schrödinger equation in the entrance and exit channels we use the two-body α - ^3He and α - ^3H central potentials of the Gaussian form from Ref. [21] as defined in Eq.(5) with the corresponding Coulomb part, see Eq.(6). For consistency we use the same parameters as in the aforementioned paper. Namely, we use $\hbar^2/2[\text{a.m.u.}] = 20.7343 \text{ MeV fm}^2$ and the Coulomb parameter $R_c = 3.095 \text{ fm}$. The experimental mass values are also taken from Ref. [21]: $m_{^4\text{He}} = A_1 \text{ a.m.u.} = 4.001506179127 \text{ a.m.u.}$, $m_{^3\text{He}} = A_2 \text{ a.m.u.} = 3.0149322473 \text{ a.m.u.}$ or $m_{^3\text{H}} = A_2 \text{ a.m.u.} = 3.0155007134 \text{ a.m.u.}$

The scattering wave function $u_E(r)$ of the relative motion is calculated as a solution of the Schrödinger equation using the Numerov method with an appropriate potential subject to the boundary condition specified in Eq.(4).

The depth parameters V_0 of the α - ^3He and α - ^3H potentials are given in Table I. All the presented potentials, including the initial deep potential V_D of Dubovichenko [21] reproduce the experimental phase shifts of α - ^3He scattering in all the partial waves and the binding energies $E_b(3/2^-) = 1.5866 \text{ MeV}$ and $E_b(1/2^-) = 1.16082 \text{ MeV}$ of the ^7Be nucleus bound states.

The width parameter of the initial potential V_D [21] was chosen as $\alpha = 0.15747 \text{ fm}^{-2}$ for all the partial waves. It yields the ANC values $C(3/2^-) = 4.34 \text{ fm}^{-1/2}$ and $C(1/2^-) = 3.71 \text{ fm}^{-1/2}$ for the bound states.

The parameters of the modified potential V_{M1} in the p-waves are fitted to reproduce the empirical values of ANC, extracted from the experimental α - ^3He scattering data given in Ref. [38] within the DWBA method, $C(3/2^-) = 4.785 \text{ fm}^{-1/2}$ and $C(1/2^-) = 4.243 \text{ fm}^{-1/2}$, while keeping the experimental phase-shift description and the binding energies. The values of the depth parameter and the width parameter α for the $p_{3/2}$ and $p_{1/2}$ bound states are given in Tables I and II, respectively. The parameters in other waves are identical to that of V_D .

In addition to the phase shifts and the binding energies, the modified potential V_{M2} is adjusted to reproduce the empirical values of ANC, extracted from the analysis of the experimental astrophysical S-factor of the $\alpha(^3\text{He}, \gamma)^7\text{Be}$ capture reaction presented in Ref.[40], $C(3/2^-) = 4.80 \text{ fm}^{-1/2}$ and $C(1/2^-) = 3.94 \text{ fm}^{-1/2}$. The values of α for the $p_{3/2}$ and $p_{1/2}$

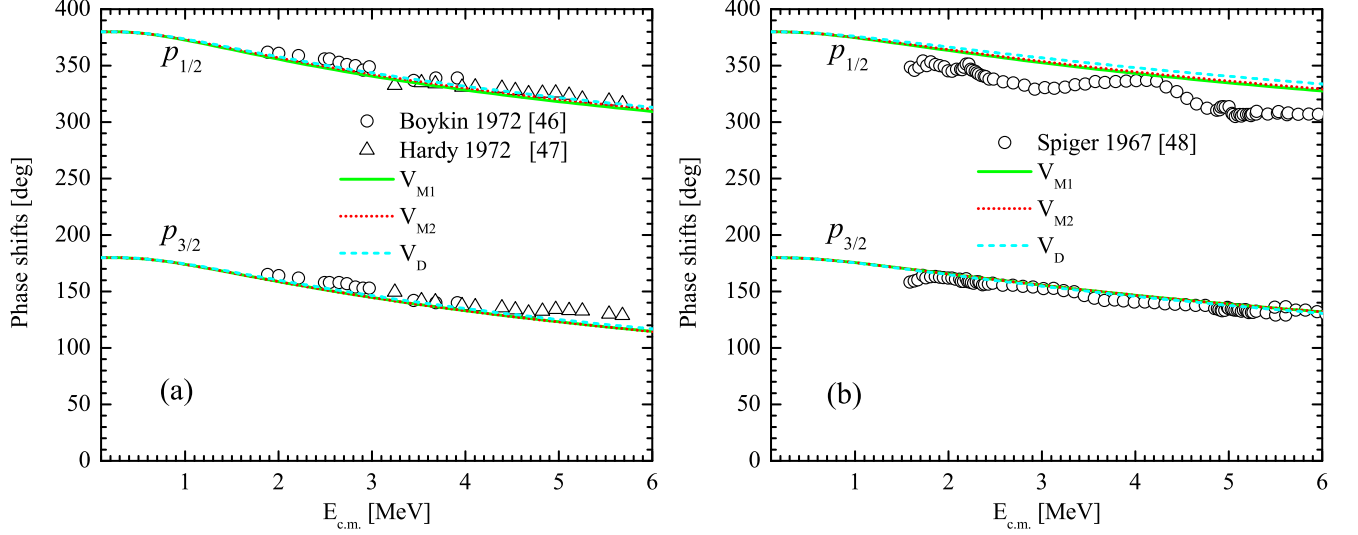


FIG. 1. p-wave phase-shift description of the ${}^3\text{He} + \alpha$ and ${}^3\text{H} + \alpha$ scattering within different potential models in comparison with available data.

bound states are given in Table II. Again the potential parameters in all the partial waves, except p-waves, are the same as in V_D and V_{M1} .

The calculated p-wave phase shifts for the ${}^3\text{He} + \alpha$ and ${}^3\text{H} + \alpha$ scattering are shown on Fig. 1 in comparison with experimental data from Refs.[46–48]. As can be seen from the figure, the modified potentials V_{M1} and V_{M2} yield equally good phase-shift description as the initial potential V_D .

As we see below, the potentials V_D , V_{M1} and V_{M2} do not reproduce the new data of the LUNA collaboration [13, 14] at energies around 100 keV and the newest data [20] at the Gamov peak $S_{34}(23_{-5}^{+6} \text{ keV}) = 0.548 \pm 0.054 \text{ keV b}$ for the astrophysical S-factor of the ${}^3\text{He}(\alpha, \gamma){}^7\text{Be}$ capture reaction. The unique property of the potential model is that there is a possibility to adjust the potential parameters in the s-wave in order to reproduce the new data for the astrophysical S-factor, while keeping the experimental phase shifts unchanged. This is possible because of the dominance of the E1-transition $s_{1/2} \rightarrow p_{3/2}$ and $s_{1/2} \rightarrow p_{1/2}$ for the capture process. The potential V_{M1}^a is obtained as a modification of the V_{M1} potential in the s-wave. Its depth and width parameter values are given in Tables I and II, respectively. The potential V_{M2}^a was obtained from V_{M2} in the same way. The modified potentials V_D^a and V_D^b are built from the original V_D potential by the modification of the s-wave parameters. The potentials V_{M1}^a , V_{M2}^a , and V_D^a are adjusted to the central value of the newest data at the

Gamov peak, while the V_D^b is adjusted to the upper limit of the error bar of the latter.

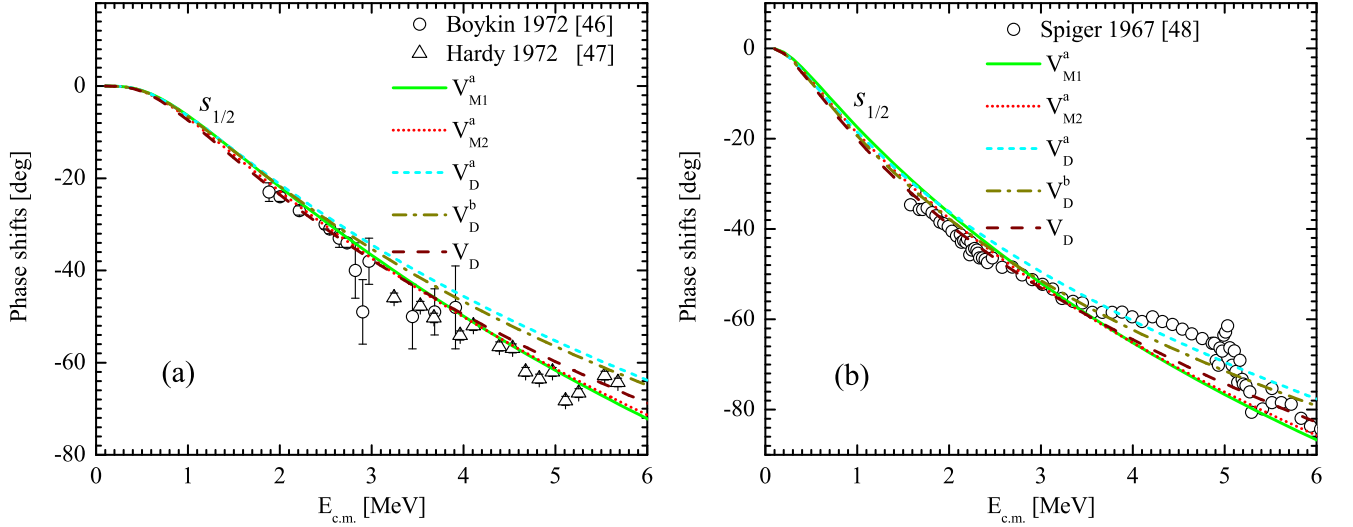


FIG. 2. s-wave phase-shift description of the ${}^3\text{He}+\alpha$ and ${}^3\text{H}+\alpha$ scattering within different potential models in comparison with available data.

The corresponding s-wave phase shift descriptions are shown in Fig. 2 for the ${}^3\text{He}+\alpha$ and ${}^3\text{H}+\alpha$ scattering. In the energy range up to 3 MeV, the modified potentials V_{M1}^a , V_{M2}^a , V_D^a and V_D^b describe the experimental data at the level of the original potential V_D .

TABLE I. Values of the depth parameter V_0 , see Eq. (5), of the $\alpha-{}^3\text{He}$ (${}^3\text{H}$) potential for different partial waves in MeV.

L_J	V_D	V_D^a	V_D^b	V_{M1}	V_{M1}^a	V_{M2}	V_{M2}^a
$s_{1/2}$	-67.5	-77.0	-130.0	-67.5	-50.0	-67.5	-54.0
$p_{1/2}$	-81.815179			-70.912	-76.680		
$p_{3/2}$	-83.589554			-75.766	-75.486		
$d_{3/2}$	-66.0						
$d_{5/2}$	-69.0						
$f_{5/2}$	-75.9						
$f_{7/2}$	-84.8						

At first step a study of the astrophysical ${}^3\text{He}(\alpha, \gamma){}^7\text{Be}$ capture process will be performed within the aforementioned potential models. At the next step, these potentials will be examined in the ${}^3\text{H}(\alpha, \gamma){}^7\text{Li}$ reaction studies with the only modification of the Coulomb

TABLE II. Values of the width parameter α , see Eq. (5), of the α - ^3He (^3H) potential for different partial waves in fm^{-2} .

L_J	V_D	V_D^a	V_D^b	V_{M1}	V_{M1}^a	V_{M2}	V_{M2}^a
$s_{1/2}$	0.15747	0.180	0.365	0.15747	0.109	0.15747	0.120
$p_{1/2}$	0.15747			0.1338	0.1463		
$p_{3/2}$	0.15747			0.1405	0.1399		
$d_{3/2}$	0.15747						
$d_{5/2}$	0.15747						
$f_{5/2}$	0.15747						
$f_{7/2}$	0.15747						

potential due to different charge values of the ^3He and ^3H nuclei. The nuclear part of the potentials will be kept unchanged on the basis of the charge-independence property of nuclear forces.

B. Estimation of the astrophysical S-factor for the $^3\text{He}(\alpha, \gamma)^7\text{Be}$ capture process

For the study of the $^3\text{He}(\alpha, \gamma)^7\text{Be}$ direct radiative capture process we first use the potentials V_D , V_{M1} and V_{M2} . As noted above, these potentials differ from each other due to the parameters used in the $p_{1/2}$ and $p_{3/2}$ partial waves and yield different values for ANC. As mentioned above, the V_{M1} and V_{M2} potentials were adjusted to the empirical ANC values from Refs. [38] and [40], respectively.

Contributions of the partial $E1$ -transition components for the $^3\text{He}(\alpha, \gamma)^7\text{Be}$ direct radiative capture process are given in the left panel of Fig. 3 for the V_{M1} potential. As can be seen from the figure, the dominant contribution in the astrophysical low energy region comes from the $E1$ -transition $s_{1/2} \rightarrow p_{3/2}$. The dominance is most prevailing at energies close to zero. At energies above 2 MeV the $E1$ -transition from the $d_{5/2}$ to the $p_{3/2}$ partial wave provides the largest contribution. Contributions of the $E2$ -components to the astrophysical S -factor within the same V_{M1} potential are shown in the middle panel of Fig. 3. The dominant contributions in low-energy region correspond to the transitions between the p-waves. A resonance behavior of the astrophysical S -factor at energies around 3 MeV is

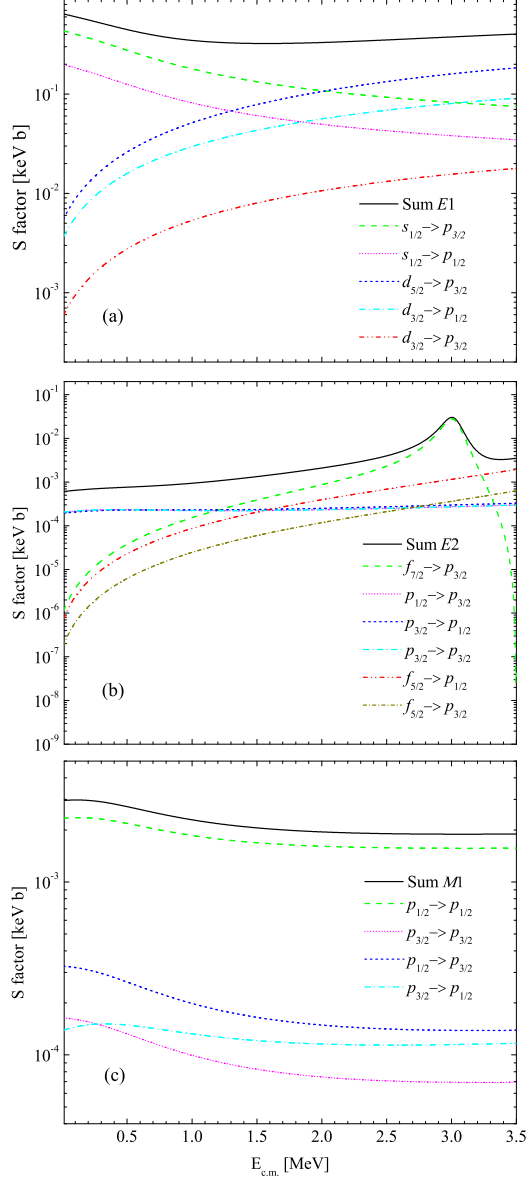


FIG. 3. Contributions of the partial $E1$ -, $E2$ - and $M1$ -components to the astrophysical S -factor for the ${}^3\text{He}(\alpha, \gamma){}^7\text{Be}$ capture process resulting from calculations with the V_{M1} potential.

well reproduced in the $f_{7/2} \rightarrow p_{3/2}$ transition. Contributions of the partial $M1$ -components to the astrophysical S -factor for the ${}^3\text{He}(\alpha, \gamma){}^7\text{Be}$ direct capture process with the same V_{M1} potential are displayed in the third panel of Fig. 3. Here the dominant contribution is the $M1$ -transition from the $p_{1/2}$ partial wave to the same one.

In order to compare the relative contributions from the electric $E1$ -, $E2$ - and magnetic $M1$ -transitions, in Fig. 4 we show the summary of the results for the astrophysical S -factor

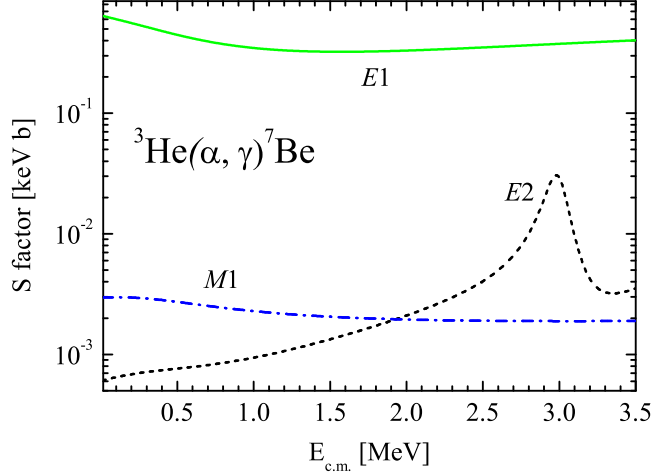


FIG. 4. Contributions of the total $E1$ -, $E2$ - and $M1$ -transitions to the astrophysical S-factor for the ${}^3\text{He}(\alpha, \gamma){}^7\text{Be}$ reaction estimated using the V_{M1} potential.

of the ${}^3\text{He}(\alpha, \gamma){}^7\text{Be}$ capture reaction calculated using the potential model V_{M1} . As can be seen from the figure, the dominance of the $E1$ -transition is maximal at the zero energy where the contribution from the electric $E1$ -transition is larger than the sum of those from the $E2$ - and $M1$ -transitions by more than two orders of magnitude.

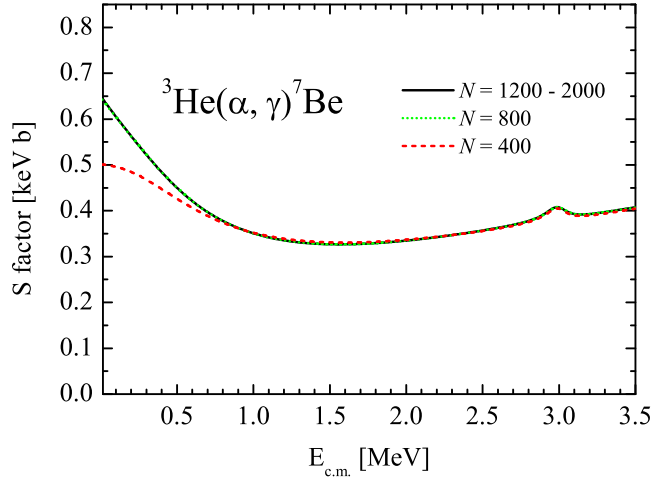


FIG. 5. Convergence of the astrophysical S-factor for the ${}^3\text{He}(\alpha, \gamma){}^7\text{Be}$ reaction with respect to the number of integration points with fixed value of $h=0.05$ fm estimated with the V_{M1} potential.

The convergence of the astrophysical S-factor with respect to the integration limit is demonstrated in Fig. 5 for the capture process ${}^3\text{He}(\alpha, \gamma){}^7\text{Be}$. As can be seen from the figure, at low astrophysical energies the convergent results are obtained with $R_{max} = 40$ fm,

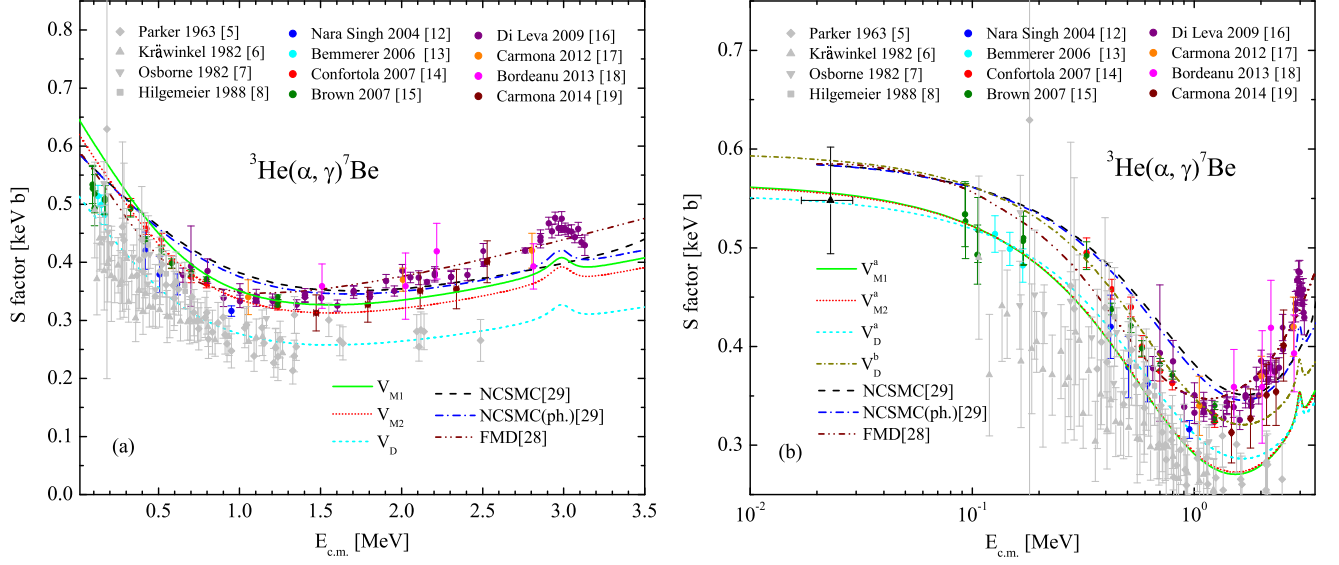


FIG. 6. Astrophysical S-factor for the ${}^3\text{He}(\alpha, \gamma){}^7\text{Be}$ synthesis reaction, estimated using different potential models in comparison with available experimental data and *ab-initio* calculations. The right panel highlights the low-energy region.

while at higher energies the convergence is reached already at $R_{max} = 20$ fm.

In Fig. 6 we show the total astrophysical S-factor for the ${}^3\text{He}(\alpha, \gamma){}^7\text{Be}$ capture reaction. The left panel of the figure displays the astrophysical S-factor of the process obtained by using the V_{M1} , V_{M2} and V_D potentials in comparison with available experimental data. As can be seen from the figure, the experimental data is well reproduced at higher energies by the V_{M1} , V_{M2} models, consistent with the NCSMC results [29]. However, these potential models overestimate the data of the LUNA collaboration [13, 14] at energies around 100 keV and the newest data [20] at the Gamov peak $S_{34}(23_{-5}^{+6} \text{ keV}) = 0.548 \pm 0.054 \text{ keV b}$. The reason is that the energy dependence of the calculated astrophysical S-factor is different from that of the microscopic NCSMC [29]. The potential model V_D substantially underestimates the astrophysical S-factor, although resulting energy dependence is similar to that obtained using the V_{M1} and V_{M2} potentials.

As we already know, the E1-transitions $s_{1/2} \rightarrow p_{3/2}$ and $s_{1/2} \rightarrow p_{1/2}$ play a dominant role in the capture process. Therefore, the potentials V_D , V_{M1} , V_{M2} can be modified and their s-wave parameters V_0 and α can be adjusted to the new data of the LUNA collaboration and the newest data at the Gamov peak. As can be seen from right panel of Fig. 6, the potentials V_D^a , V_{M1}^a , V_{M2}^a describe well the astrophysical S-factor at low energies, however they have

an increasing tendency to underestimate the data above 0.5 MeV. As discussed later, this underestimation is not present for the mirror reaction. A reason for the underestimation is that the potential model can not describe the coupling to different inelastic channels, like ${}^6\text{Li}+p$ for the process ${}^3\text{He}(\alpha, \gamma){}^7\text{Be}$ or ${}^6\text{Li}+n$ for the mirror capture process ${}^3\text{H}(\alpha, \gamma){}^7\text{Li}$. The main role in the coupling to inelastic channels is played by the Coulomb forces and therefore the coupling should be important for the first process. Also, tensor forces between valence nucleons should play some role. These give rise to larger contribution of higher partial waves of relative motion between valence nucleons.

The modified V_D^b potential, whose s-wave parameters were fitted to the upper limit of the newest data at the Gamov peak [20], yields a description of the experimental data in both low and higher energy region with the same quality which is not as good as for the V_D^a , V_{M1}^a , V_{M2}^a potentials.

As can be noted from the last figure, the energy dependence of the astrophysical S-factor for the potential model slightly differs from that resulting from the ab-initio study in the NCSMC [29] and is substantially different from energy dependence of the fermionic molecular dynamics (FMD) model [28] for the capture process. The reason could be due to the fact that the experimental s-wave phase shifts are not well reproduced by the NCSMC model. A significantly different energy behavior of the FMD model and the potential approach could reflect the fact that the inputs of the models are quite different. The FMD model is a microscopic approach based on a realistic effective interaction that reproduces the nucleon-nucleon scattering data. At the same time, the potential approach is based on the effective $\alpha+{}^3\text{He}$ (${}^3\text{H}$) interaction potentials adjusted to the bound state properties of the ${}^7\text{Be}$ nucleus and $\alpha+{}^3\text{He}$ scattering data.

The nodal positions of the s-wave scattering and the p-wave bound state wave functions at small distances, which are due to orthogonality to the Pauli forbidden states (two in s-wave and one in each of the $p_{1/2}$ and $p_{3/2}$ partial waves), play a crucial role in the description of the astrophysical S-factor. They significantly affect the values of the overlap integral of the initial and final state wave functions. A modification of the potential parameters in the s- and p-waves is equivalent to shifting the nodal positions of the s-wave scattering and p-wave bound state wave functions. Thus the role of the Pauli forbidden states in the capture process is similar to the important part they play in the beta-decay process of the ${}^6\text{He}$ halo nucleus [41, 42] and M1-transition of the ${}^6\text{Li}(0^+)$ [49] isobar-analog state to the

$\alpha - d$ two-body continuum.

C. Estimation of the astrophysical S-factor for the ${}^3\text{H}(\alpha, \gamma){}^7\text{Li}$ capture process

As mentioned above the same V_d , V_{M1} , V_{M2} potential models and their modifications V_D^a , V_{M1}^a , V_{M2}^a , V_D^b in the s-wave are used for the study of the mirror capture reaction ${}^3\text{H}(\alpha, \gamma){}^7\text{Li}$. The Coulomb part of these potentials, defined in Eq. (6), is modified according to the charge value of the ${}^3\text{H}$ cluster $Z=1$. As demonstrated above, the phase shifts in the $s_{1/2}$, $p_{1/2}$, $p_{3/2}$, $d_{3/2}$, $d_{5/2}$, $f_{5/2}$ and $f_{7/2}$ partial waves, and the binding energies $E_b(3/2^-)=2.467$ MeV and $E_b(3/2^-)=1.990$ MeV of the bound states are well reproduced.

Partial contributions of the $E1$ -, $E2$ - and $M1$ -transitions to the astrophysical S-factor for the mirror ${}^3\text{H}(\alpha, \gamma){}^7\text{Li}$ reaction show the same behavior as for the process ${}^3\text{He}(\alpha, \gamma){}^7\text{Be}$.

In Fig. 7 we show total contributions of the $E1$, $E2$ and $M1$ transitions to the astrophysical S-factor for the ${}^3\text{H}(\alpha, \gamma){}^7\text{Li}$ synthesis reaction calculated with the V_{M1} potential model. As can be seen, the dominant role of the $E1$ -transition remains.

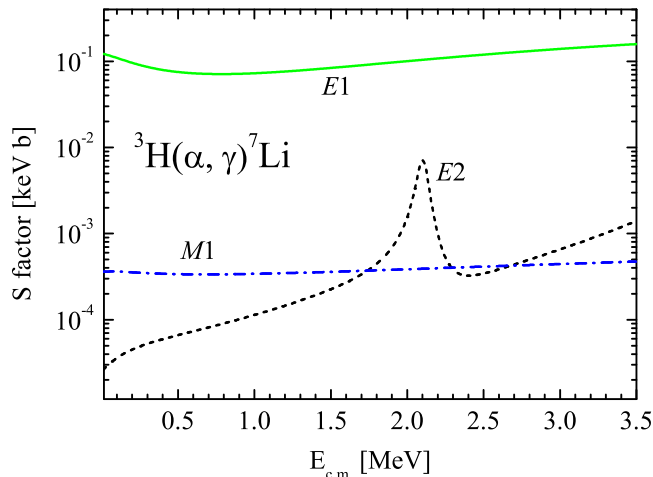


FIG. 7. Contributions of the $E1$, $E2$ and $M1$ transitions to the astrophysical S-factor for the ${}^3\text{H}(\alpha, \gamma){}^7\text{Li}$ synthesis reaction calculated with the V_{M1} potential.

Finally, Figure 8 presents the total astrophysical S-factor for the ${}^3\text{H}(\alpha, \gamma){}^7\text{Li}$ reaction calculated with the different potentials in comparison with available experimental data. Since the latest data set [11] dates back to 1994, it is difficult to make any conclusion on the experimental precision. Nevertheless, one can see from the figure that the V_D , V_{M1}^a , V_{M2}^a potentials

are more consistent with the experimental data than the NCSMC [29] and FMD [28] models. As in the case of the ${}^3\text{He}(\alpha, \gamma){}^7\text{Be}$ reaction, the energy dependence of the astrophysical S-factor with the potential model is close to that with the NCSMC model but substantially different from the FMD model. Even more importantly, the V_{M1}^a , V_{M2}^a potentials reproduce well both energy dependence and normalization of the latest experimental data. This means that a coupling to the inelastic channel ${}^6\text{Li}+n$ for the mirror capture process ${}^3\text{H}(\alpha, \gamma){}^7\text{Li}$ is not important unlike the coupling to the ${}^6\text{Li}+p$ channel in the ${}^3\text{He}(\alpha, \gamma){}^7\text{Be}$ capture process. As was noted earlier, the main role in the couplings to inelastic channels belongs to Coulomb forces which are not present in the ${}^6\text{Li}+n$ channel.

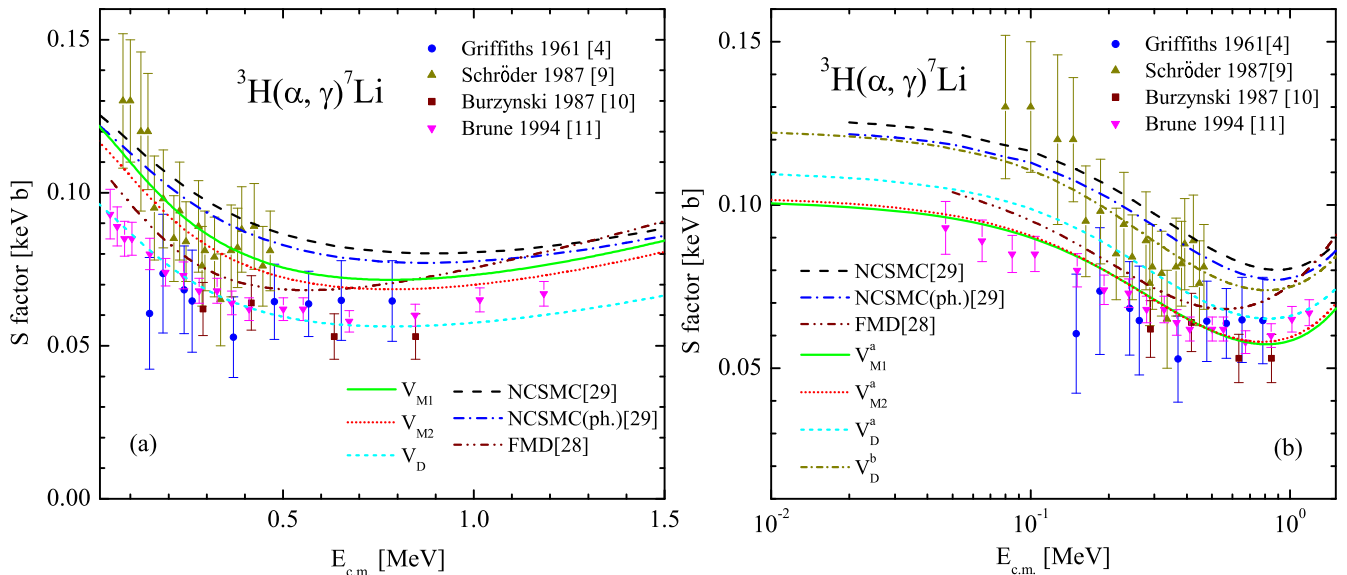


FIG. 8. Astrophysical S-factor for the ${}^3\text{H}(\alpha, \gamma){}^7\text{Li}$ synthesis reaction calculated with different potentials in comparison with available experimental data and *ab-initio* calculations.

IV. CONCLUSIONS

The astrophysical ${}^3\text{He}(\alpha, \gamma){}^7\text{Be}$ and ${}^3\text{H}(\alpha, \gamma){}^7\text{Li}$ direct capture processes have been studied in the two-body potential model. Central potentials of a simple Gaussian form with the appropriate Coulomb part, which reproduce the α - ${}^3\text{He}$ phase shifts in all the partial waves and binding energies of the ${}^7\text{Be}$ ground $3/2^-$ and first excited $1/2^-$ states, have been tested. It is important to note that the potentials, adjusted to the properties of the ${}^7\text{Be}$ nucleus in this way, were able to reproduce the properties of the ${}^7\text{Li}$ nucleus, phase shifts in the partial

waves and the binding energies of the ground $3/2^-$ and first excited $1/2^-$ states.

In addition, the potentials in the p-waves were adjusted to reproduce the empirical values of the ANC for the $\alpha-^3\text{He}$, extracted from the phase-shift analysis and alternatively, from the analysis of the astrophysical S-factor available in the literature.

It has been shown that the E1-transition from the initial s-wave to the final p-waves is strongly dominant in both capture reactions considered in this work. On this basis we adjust the s-wave potential to reproduce the new data of the LUNA collaboration around 100 keV and the latest data at the Gamov peak obtained on the basis of the observed neutrino fluxes from the Sun, $S_{34}(23_{-5}^{+6} \text{ keV})=0.548\pm 0.054 \text{ keV b}$ for the astrophysical S-factor of the capture process $^3\text{He}(\alpha, \gamma)^7\text{Be}$. The resulting model describes well the experimental data at low energies, however has an increasing tendency to underestimate the data above 0.5 MeV. The underestimation could be due to the coupling to the inelastic $^6\text{Li}+p$ channel, which can not be taken into account in the developed potential model approach. It is found that the energy dependence of the potential model is slightly different from that of the microscopic no-core shell model with continuum (NCSMC) and substantially differs from that of the fermionic molecular dynamics (FMD) model.

It is also shown that the experimental data for the mirror astrophysical $^3\text{H}(\alpha, \gamma)^7\text{Li}$ capture reaction can be well described in the potential model. The successful description of the data for the mirror process is suggested to be due to a negligible role of the coupling to the $^6\text{Li}+n$ inelastic channel in which the Coulomb forces are not present.

In conclusion, the V_{M1}^a , V_{M2}^a potential models which were fitted to the new data of the LUNA collaboration for the astrophysical S-factor of the $^3\text{He}(\alpha, \gamma)^7\text{Be}$ capture process by the modifying the s-wave $\alpha-^3\text{He}$ nuclear interaction potential describe well this capture process in the BBN energy region (180-400 keV). Additionally, they yield very good description of the latest experimental data for the $^3\text{H}(\alpha, \gamma)^7\text{Li}$ mirror capture process. From the beginning, these models describe well bound state (binding energies and ANC) and scattering state (phase shifts) properties of both $\alpha+^3\text{He}$ and $\alpha+^3\text{H}$ systems.

ACKNOWLEDGMENTS

A.S.K acknowledges support from the Australian Research Council and partial support from the U.S. National Science Foundation under Award No. PHY-1415656. We would like

to thank J. Dohet-Eraly for providing us with the results of Ref. [29] for the astrophysical S-factor in a tabulated form.

-
- [1] E. G. Adelberger *et al.*, Rev. Mod. Phys. **83**, 195 (2011).
 - [2] B. D. Fields, Annual Review of Nuclear and Particle Science **61**, 47 (2011).
 - [3] M. Asplund, D. L. Lambert, P. E. Nissen, F. Primas, and V. V. Smith, The Astrophysical Journal **644**, 229 (2006).
 - [4] G. M. Griffiths, R. A. Morrow, P. J. Riley, and J. B. Warren. Can. J. Phys. **39**, 1397 (1961).
 - [5] P. D. Parker and R. W. Kavanagh. Phys. Rev. **131**, 2578 (1963).
 - [6] H. Kräwinkel, H.W. Becker, L. Buchmann, J. Görres, K. U. Kettner, *et al.*, Z. Phys. **A 304**, 307 (1982).
 - [7] J. L. Osborne, C. A. Barnes, R. W. Kavanagh, R. M. Kremer, G. J. Mathews, J. L. Zyskind, P. D. Parker, and A. J. Howard. Phys. Rev. Lett. **48**, 1664 (1982).
 - [8] M. Hilgemeier, H. W. Becker, C. Rolfs, H. P. Trautvetter, and J. W. Hammer. Z. Phys. **A 329**, 243 (1988).
 - [9] U. Schröder, A. Redder, C. Rolfs, R. E. Azuma, L. Buchmann, C. Campbell, J. D. King, and T. R. Donoghue. Phys. Lett. **B 192**, 55 (1987).
 - [10] S. Burzyński, K. Czerski, A. Marcinkowski, and P. Zupranski. Nucl. Phys. **A 473**, 179(1987).
 - [11] C. R. Brune, R.W. Kavanagh, and C. Rolfs. Phys. Rev. **C 50**, 2205 (1994).
 - [12] B. S. Nara Singh, M. Hass, Y. Nir-El, and G. Haquin. Phys. Rev. Lett. **93**, 262503 (2004).
 - [13] D. Bemmerer, F. Confortola, H. Costantini, A. Formicola, Gy. Gyürky, *et al.*, Phys. Rev. Lett. **97**, 122502 (2006).
 - [14] F. Confortola, D. Bemmerer, H. Costantini, A. Formicola, Gy. Gyürky, *et al.*, Phys. Rev. **C 75**, 065803 (2007).
 - [15] T.A. D. Brown, C. Bordeanu, K. A. Snover, D. W. Storm, D. Melconian, A. L. Sallaska, S. K. L. Sjue, and S. Triambak. Phys. Rev. **C 76**, 055801 (2007).
 - [16] A. Di Leva, L. Gialanella, R. Kunz, D. Rogalla, D. Schürmann, *et al.*, Phys. Rev. Lett. **102**, 232502 (2009).
 - [17] M. Carmona-Gallardo, B. S. Nara Singh, M. J. G. Borge, J. A. Briz, M. Cubero, *et al.*, Phys. Rev. **C 86**, 032801 (2012).

- [18] C. Bordeanu, Gy. Gyürky, Z. Halász, T. Szücs, G. G. Kiss, Z. Elekes, J. Farkas, Zs. Fülöp, and E. Somorjai. Nucl. Phys. **A 908**, 1 (2013).
- [19] M. Carmona Gallardo. Ph.D. thesis, Universidad Complutense de Madrid, Madrid, 2014.
- [20] M.P. Takacs, D. Bemmerer, T. Szücs, and K. Zuber. Phys. Rev. D **91**, 123526 (2015).
- [21] S.B. Dubovichenko, Physics of Atomic Nuclei, **73**, 1526 (2010).
- [22] P. Mohr, Phys. Rev. C **79**, 065804 (2009)
- [23] A. Mason, R. Chatterjee, L. Fortunato, and A. Vitturi, Eur. Phys. J. **A39**, 107 (2009).
- [24] P. Descouvemont and D. Baye, Rep. Prog. Phys. **73**, 036301 (2010).
- [25] T. Kajino, Astrophysics J. **319**, 531 (1987).
- [26] V. S. Vasilevsky, A. V. Nesterov, and T. P. Kovalenko, Physics of Atomic Nuclei, **75**, 818 (2012).
- [27] A.S. Solovyev, S.Yu. Igashov, Yu.M. Tchuvil'sky, J. Phys. CS **569**, 0122020 (2014).
- [28] T. Neff, Phys.Rev.Lett. **106**, 042502 (2011).
- [29] J. Dohet-Eraly, P. Navratil, S. Quaglioni, W. Horiuchi, G. Hupin and F. Raimondi, Phys.Lett. B, **757**, 430 (2016).
- [30] K.M. Nollett, Phys.Rev. C **63**, 054002 (2001).
- [31] P. R. Fraser, K. Massen-Hane, A.S. Kadyrov, K. Amos, I. Bray, and L. Canton, Phys. Rev. C **96**, 014619 (2017).
- [32] E.M. Tursunov, S.A. Turakulov, P. Descouvemont. Phys. Atom. Nucl., **78**, 193 (2015).
- [33] E.M. Tursunov, A.S. Kadyrov, S.A. Turakulov and I.Bray, Phys. Rev. C **94**, 015801 (2016).
- [34] L.D. Blokhintsev, V.I. Kukulín, A.A. Sakharuk, D.A. Savin, and E.V. Kuznetsova, Phys. Rev. C **48**, 2390 (1993).
- [35] J.-M. Sparenberg, P. Capel, and D. Baye, Phys. Rev. C **81**, 011601 (2010).
- [36] L.D. Blokhintsev, A.S. Kadyrov, A.M. Mukhamedzhanov and D. A. Savin Phys. Rev. C **95**, 044618 (2017).
- [37] L.D. Blokhintsev, A.S. Kadyrov, A.M. Mukhamedzhanov and D. A. Savin Phys. Rev. C **97**, 024602 (2018).
- [38] R. Yarmukhamedov, O.R. Tojiboev, and S.V. Artemov, Nuovo Cimento **C 39**, 364 (2016).
- [39] A.M. Mukhamedzhanov, Shubhchintak, and C.A. Bertulani, Phys. Rev. C **93**, 045805 (2016).
- [40] Q.I. Tursunmahatov, R. Yarmukhamedov, Phys. Rev. C **85**, 045807 (2011).
- [41] E.M. Tursunov, D. Baye and P. Descouvemont, Phys. Rev. C **73**, 014303 (2006).

- [42] E.M. Tursunov, D. Baye and P. Descouvemont, Phys. Rev. **C74** 069904 (2006).
- [43] C. Angulo, M. Arnould, M. Rayet et al. Nucl. Phys. **A656**, 3 (1999).
- [44] A.M. Mukhamedzhanov, L.D. Blokhintsev, and B.F. Irgaziev, Phys. Rev. **C 83**, 055805 (2011).
- [45] W.A. Fowler, G.R. Gaughlan and B.A. Zimmerman, Annu. Rev. Astron. Astrophys. **13**, 69 (1975).
- [46] W.R. Boykin, S.D. Baker, D.M. Hardy, Nucl. Phys. **A195**, 241 (1972).
- [47] D.M. Hardy, R.J. Spiger, S.D. Baker, Y.S. Chen, T.A. Tombrello, Nucl. Phys. **A195**, 250 (1972).
- [48] R.J. Spiger and T.A. Tombrello, Phys. Rev. **163**, 964 (1967)
- [49] E.M. Tursunov, P. Descouvemont and D. Baye, Nucl. Phys. **A793**, 52 (2007).